Proceeding of the IEEE
International Conference on Robotics and Biomimetics
Dali, China, December 2019

3-D Motion Analysis and Implementation of a Developed Gliding Robotic Dolphin

Jian Wang[1,2], Zhengxing Wu[1,2], Jincun Liu[3], Min Tan[1,2], and Junzhi Yu[1,3]
[1]*State Key Lab Management and Control for Complex Systems, Institute of Automation, CAS, Beijing 100190, China*
[2]*University of Chinese Academy of Sciences, Beijing 100049, China*
[3]*Dept. Mech. Eng. Sci., BIC-ESAT, College of Engineering, Peking University, Beijing 100871, China*
{*wangjian2016, zhengxing.wu, min.tan, junzhi.yu*}*@ia.ac.cn, liujincun@pku.edu.cn*

***Abstract*—This paper investigates the three-dimensional (3-D) maneuverability of a gliding robotic dolphin through analyzing the horizontal and vertical motions. Concretely, in order to improve the performance in the horizontal plane, the gliding robotic dolphin is developed with a rudder installed on its belly, and the 3-D full-state dynamic model is derived briefly. By setting two typical body and/or caudal fin (BCF)-based and three typical median and/or paired fin (MPF)-based turning patterns, the turning performances are revealed and analyzed. With regard to the vertical plane, a novel finite state machine framework is proposed to realize the vertical downward action. Finally, extensive experiments involving the turning and vertical motions are conducted to illustrate and analyze the 3-D maneuverability, which provides valuable guidance for the real-world applications of the gliding robotic dolphin.**

***Index Terms*—Gliding robotic dolphin, motion analysis, turning patterns, vertical action.**

I. Introduction

In recent years, ocean exploration has attracted much attention of many researchers due to its abundant mineral resources, biological resources, and energy. Therefore, the autonomous underwater vehicles (AUVs) have made a more significant influence. Compared with the traditional AUVs, various bio-inspired underwater robots have aroused more interest owing to their high-maneuverability and high-efficiency swimming styles [1], [2], [3]. Among these prototypes, the robotic dolphin can perform many astonishing motions with high maneuverability, such as the leaping action [4] and 360° frontflip-backflip motion [5]. Nevertheless, these motions may consume much energy simultaneously, which greatly shortens the endurance time of the robotic dolphin. Hence, thanks to the advantages of traditional underwater gliders with low energy consumption [6], [7], the first prototype of the gliding robotic dolphin was designed through combining the robotic dolphins with traditional underwater gliders [8], [9]. Next, the gliding robotic dolphin was developed to 1.5 m long, based on which the heading and pitch control with rotatable surfaces were addressed [10], [11].

Three-dimensional (3-D) maneuverability has always been a considerable topic for underwater robots. Relying on their highly developed muscle structure, the natural dolphins can easily realize an 11-m/s swimming speed, and a 0.20-body-lengths (BL) turn radius [12]. However, restricted to the mechanical structure, the robotic dolphin has poor relatively maneuverability in yaw motion. As a consequence, Cao *et al.* designed a robotic dolphin with one turning joint, and realized the noticeable heading control based on a self-tuning fuzzy strategy [13], but this design occupied a relatively large internal space. Liu *et al.* studied the median and/or paired fin (MPF)-based turning patterns and achieved little-radius turning under the differential flapping way of bilateral flippers [14]. Nevertheless, the robotic dolphin swims with lower speed under the MPF mode than that under body and/or caudal fin (BCF) mode, which leads to weak anti-interference ability. Therefore, the BCF-based turning motion should be also further studied. Concerning the vertical motion, the gliding angle of traditional underwater gliders is usually adjusted by buoyancy-driven and centroid systems. Rely on the high maneuverability of dolphin-like motion, the gliding robotic dolphin is adjusted to a fixed attitude, then the gliding motion can be started to attain larger gliding angle.

The main objective of this paper is to study the horizontal and vertical motions of a gliding robotic dolphin to further obtain more flexible and precise 3-D maneuvers, which can lay the foundation for practical applications. Compared with previous work, the main contributions of this work conclude two aspects. First, a rudder is newly installed on the belly of the gliding robotic dolphin to improve turning ability. Then, based on the developed platform, five turning motions including both the BCF and MPF modes are investigated and analyzed. Second, a novel framework with finite state machine is proposed to achieve vertical downward action, further to realize gliding motion with a large gliding angle. Extensive experiments including the horizontal and vertical motions are carried out to illustrate the 3-D maneuverability.

The rest of this paper is organized as follows. In Section II, the mechanical design and dynamic model of a gliding

*This work was supported in part by the National Natural Science Foundation of China under Grant 61421004, Grant 61836015, Grant 61633020, Grant 61633017, and Grant 61603388, and in part by the Key Project of Frontier Science Research of Chinese Academy of Sciences (Grant No. QYZDJ-SSW-JSC004).

978-1-7281-6321-5/19//$31.00 ©2019 IEEE

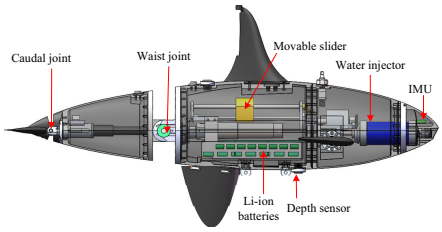

(a)

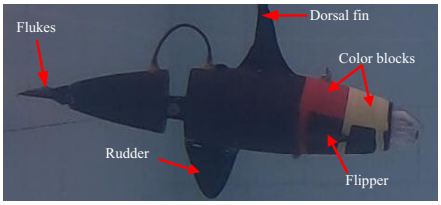

(b)

Fig. 1. Overview of the gliding robotic dolphin (a) Mechanical structure; (b) Prototype.

robotic dolphin are briefly offered. Section III provides the detailed 3-D motion setup and analysis. The experimental results as well as analyses are presented in Section IV. Finally, conclusions and future work are summarized in Section V.

II. Mechanical Design and Dynamic Model

A. Mechanical Design

Fascinated by high maneuverability of cetaceans, the gliding robotic dolphin is modeled after the killer whale for streamlined shape. Fig. 1 illustrates the mechanical structure and robotic prototype. As is shown, the gliding robotic dolphin is composed of dolphin-like and gliding parts. Concretely, the dolphin-like part mainly consists of the BCF and MPF propulsive mechanisms. The former is constituted with the waist and caudal joints, which is driven by Maxon motors (RE30 and EC16). As for the latter, two servo motors named Hitec-HS7980 are employed to drive flippers. Regarding the gliding parts, the buoyancy and centroid adjustments are actuated via a RE16-driven water injector and a RE13-driven slider mass, respectively. Besides, there are some onboard sensors installed inside the robot. The attitude and depth information can be attained by a nine-axis inertial measurement unit (IMU) and a pressure sensor, respectively.

B. Dynamic Model

In this subsection, based on our previous work [15], a brief derivation of the full-state dynamic model including the dolphin-like and gliding motions is presented. Firstly, some coordinate systems including the global framework $C_g = o_g x_g y_g z_g$, a body framework $C_b = o_b x_b y_b z_b$, and fin surfaces frameworks are established as shown in Fig. 2. Compared with the previous model, the rudder is newly added. Hence, the fin surfaces frameworks are illustrated as

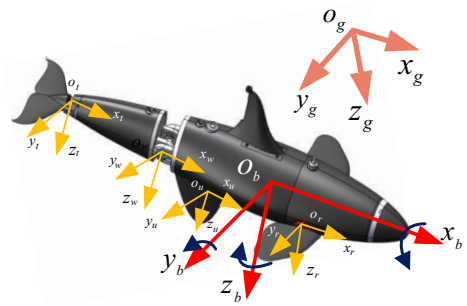

Fig. 2. Coordinate systems including the inertial, body, and fin frames.

$C_i = o_i x_i y_i z_i$, and $i = w,t,l,r,u$ indicate the waist, flukes, left flipper, right flipper, and rudder, respectively.

By defining the velocity vectors with respect to (w.r.t.) the global framework $V_g = ({U_g}^T, {\Omega_g}^T)^T$ and w.r.t. the body framework $V_b = ({U_b}^T, {\Omega_b}^T)^T$, the kinematic model can be derived as follows

$$\begin{aligned} V_g &= J_1 V_b \\ \Omega_g &= J_2 \Omega_b \end{aligned} \tag{1}$$

where J_1 and J_2 denote the transform matrix from C_b to C_g.

Take the consideration of the rotatable surfaces, their own kinematics are followed by

$$\begin{aligned} V_i &= {}^i H_b V_b + \delta_i \qquad (i = w,l,r) \\ V_t &= {}^t H_w V_w + \delta_t \\ V_u &= {}^u H_b V_b \end{aligned} \tag{2}$$

where ${}^i H_b (i = w,l,r,u)$ and ${}^t H_w$ illustrate (6×6) transformation matrix, and δ_i denotes the angular velocity vector. Note that the rudder can be just deflected to a certain angle, which is different from rotatable surfaces.

Thereafter, according to (2), we can obtain the speed derivative. Next, combining with the hydrodynamic analyses, the full-state dynamic model for the dolphin-like and gliding motions can be computed by Newton's law

$$M\dot{V}_b = -\Pi_e + \Pi_c + \Pi_h + \Pi_g + \Gamma_m + \Gamma_j \tag{3}$$

where

$$\begin{aligned} M &= \sum_{i=b,w,t,l,r,u} {}^b H_i M_i {}^i H_b \\ \Pi_c &= -\sum_{i=b,w,t,l,r,u} {}^b H_i \Gamma_{ci} \\ \Pi_h &= \sum_{i=b,w,t,l,r,u} {}^b H_i \Gamma_{hi} \\ \Pi_g &= G_b \\ \Gamma_m &= m_m \begin{pmatrix} 2\hat{\dot{P}}_m \Omega_b - \ddot{P}_m \\ \hat{P}_m (2\hat{\dot{P}}_m \Omega_b - \ddot{P}_m) \end{pmatrix} \\ \Gamma_j &= m_j \begin{pmatrix} 2\hat{\dot{P}}_j \Omega_b - \ddot{P}_j \\ \hat{P}_j (2\hat{\dot{P}}_j \Omega_b - \ddot{P}_j) \end{pmatrix} \end{aligned}$$

where Γ_j and Γ_m represent the forces and torque generated by water injector and movable slider, respectively; Γ_{hi} indicates hydrodynamic force and torque of part i; Γ_{bi} is the external force of body acting on the i part; Thus, Γ_{ib} illustrates the external forces of part i on body, and there exists the same explanation for Γ_{wt}. Besides, $G_b = (G_n, \tau_n)^T$ denotes the net buoyancy force and torque, and the total inertia matrix is defined as M_i $(i = b, w, t, l, r, u)$. P_i represents the position vectors of part i.

III. 3-D Motion Setup and Analysis of the Gliding Robotic Dolphin

A. Horizontal Motion

For the robotic dolphin, the flippers are the only turning mechanisms that can provide yaw moment. However, the thrust generated by flippers is relatively deficient, which directly leads to the poor anti-interference ability. In practical applications, it is apt for the gliding robotic dolphin to apply the MPF-based turning modes in a narrow area. Conversely, the robot can achieve high speed under BCF motion. By virtue of the single flipper's deflection, the robot can steer in BCF motion. Nevertheless, the turning performances are unsatisfactory just via the flippers, such as low turning rate and large turning radius, the reason for which may lie in two aspects. On one hand, the flipper's water supply area is not big enough to generate large hydrodynamic force. On the other hand, the flippers locate at the closer position to the center of gravity, and are not along the axis of the body. Thereby, a rudder owning the similar shape as flippers' is newly designed to install on the belly of the gliding robotic dolphin to improve the turning ability. Combining the rudder with flipper, we propose five turning modes including the two typical BCF-based and three typical MPF-based turning patterns, as illustrated in Fig. 3. The two-way arrow in Fig. 3 indicates that the joint can continuously flapping, while the one-way arrow illustrates that the joint can only deflect to a fixed angle. The detail introductions of five modes are taken as follows.

1) BCF-based mode: The first mode labeled as M1 is just on the basis of the rudder to obtain yaw moment. Meanwhile, the waist and caudal joints are driven by central pattern generators (CPG) model. When the rudder is deflected to a negative angle, the gliding robotic dolphin will acquire the yaw moment to turn right. Further, the flipper joins in the turning task in the second mode M2. Obviously, if the right flipper is deflected to $-90°$, the robot can get larger yaw moment. Hence, combining the flipper with rudder, the turning ability can be significantly improved.
2) MPF-based mode: The third and fourth modes are nearly the same as the first and second ones, other than that the BCF mode is replaced by the MPF mode of the unilateral flipper. As for the fifth mode M5, the robot flaps two flippers simultaneously, in which the right flipper is deflected to $180°$ first. Via differential flapping of bilateral flippers, the two flippers can generate reverse direction hydrodynamic forces, and thereby the robot can steer with a quiet little radius.

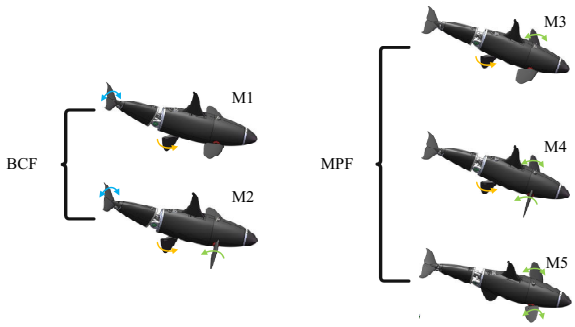

Fig. 3. The schematic diagram of five turning motions.

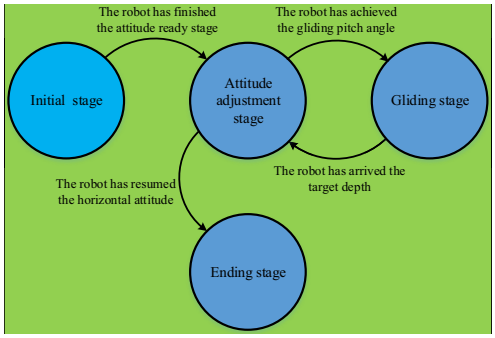

Fig. 4. The finite state machine of the vertical motion.

In theory, the turning radius with BCF-based turning mode may be larger than that with MPF-based mode, the main reason for which is that the forward speed of BCF mode is significantly greater. Specially, it is worthwhile to mention that we just conduct the experiments in which the robot turns around clockwise due to the limitation of small test pool. Regarding the counterclockwise turning motion, the conditions are the same owing to the symmetry of mechanical mechanism.

B. Vertical Motion

High maneuverability in the vertical plane is of crucial importance for the AUVs to realize efficient 3-D motion. Thanks to the powerful pitch adjustment capability of the propulsive mechanism, the robotic dolphin has a natural advantage in the vertical motion. Furthermore, with the support of the gliding parts, the gliding robotic dolphin owns stronger ability to accomplish trickier tasks in real-world applications through combination of the dolphin-like and gliding motions. For traditional AUVs, the ways of vertical motion are mostly subject to insufficient maneuverability. Therefore, we propose a finite state machine (FSM) framework to realize the gliding

motion with large gliding angle, as illustrated in Fig. 4. There are 4 stages in the FSM framework.

1) Initial stage: In this stage, the robot does some preparatory works including the initialization of buoyancy-driven, centroid and propulsive systems. When the pitch angle exceeds a threshold, the system will enter the next stage.
2) Attitude adjustment stage: The task of this stage is to change the attitude rapidly with the help of propulsive system. Hence, there are two conditions at this stage. On one hand, when the initialization is finished, the BCF mode is started up with CPG offset to adjust the pitch angle. Note that we need to add the offset β_i to output angle since we choose the unilateral oscillators as the CPG model output [17], i.e. $y_i = \psi_i + \beta_i$. ψ_i indicates the output angle calculated by CPG. On the other hand, when the robot glides to a target depth or has to glides up, the robot will adjust to horizontal or vertical upward attitude, and the stage will be executed.
3) Gliding stage: When obtaining a larger pitch angle, the robot can switch to the gliding stage. In this stage, the robot can exert the closed-loop control to keep larger gliding angle.
4) Ending stage: When the robot has adjusted to the target attitude after the second stage, the vertical motion has been completed. The next task can be carried out further.

IV. Experimental Results

To assess the 3-D motion performances of the gliding robotic dolphin, extensive experiments are conducted in a 1.1 m depth test pool. In particular, through identifying the color block on the gliding robotic dolphin, a global camera system is employed to measure its motion. Besides, the simulations are run on MATLAB/SIMULINK based on the established dynamic model in Section II, and the simulation conditions are tabulated in [15].

A. Experiments of Horizontal Motion

In this subsection, we designed four sets including the rudder angle δ_u, flipper angle δ_f, and flapping frequency of two modes f_b, f_m, which took the forms as

$$\begin{cases} \Delta_U = \{0^\circ,\ 30^\circ,\ 45^\circ,\ 60^\circ\} \\ \Delta_F = \{0^\circ,\ 90^\circ\} \\ F_B = \{1 \text{ Hz},\ 1.5 \text{ Hz},\ 2 \text{ Hz}\} \\ F_M = \{1.5 \text{ Hz},\ 2 \text{ Hz},\ 2.5 \text{ Hz}\} \end{cases} \tag{4}$$

1) BCF-based turning mode: The experimental results are plotted in Fig. 5, in which Fig. 5(a) represents the data under different δ_u and δ_f. The data on the left side of Fig. 5(a) shows the robot's trajectory, from which we can draw some conclusions. First, when combining the rudder with flipper, the turning radii were much smaller than using either one. Second, the turning performance was better when $\delta_u = 45^\circ$,

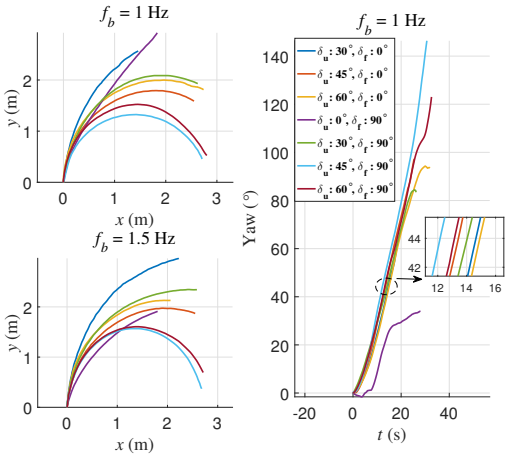

(a)

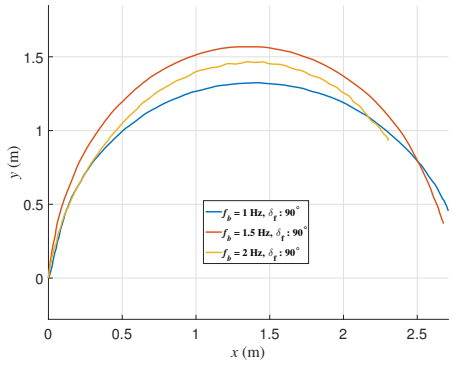

(b)

Fig. 5. Experimental data of turning mode based on BCF. (a) Under different rudder angle; (b) Under different CPG frequency.

the main reasons for which may lied in larger water supply area than than in the condition of $\delta_u = 30^\circ$, and relatively higher speed than in $\delta_u = 60^\circ$. As for the trajectory when $f_b = 1.5$ Hz, $\delta_u = 0^\circ$, $\delta_f = 90^\circ$, it seemed that the robot occured deflection earlier, the reason for which was the non-zero initial yaw angle. As expected, it owned a lower turning rate in the latter stage. Regarding the yaw angle, we could conclude the order of average turning rate

$$W_{\delta_u=45^\circ,\delta_f=90^\circ} > W_{\delta_u=60^\circ,\delta_f=90^\circ} > W_{\delta_u=45^\circ,\delta_f=0^\circ} > W_{\delta_u=30^\circ,\delta_f=90^\circ} > W_{\delta_u=30^\circ,\delta_f=0^\circ} > W_{\delta_u=60^\circ,\delta_f=0^\circ}$$

and when $\delta_u = 0^\circ$, $\delta_f = 90^\circ$, the turning performance was poor. Of course, the factors influencing the turning rate were manifold, such as the forward speed and swimming attitude. The general order could provide a theoretical basis for further deep research.

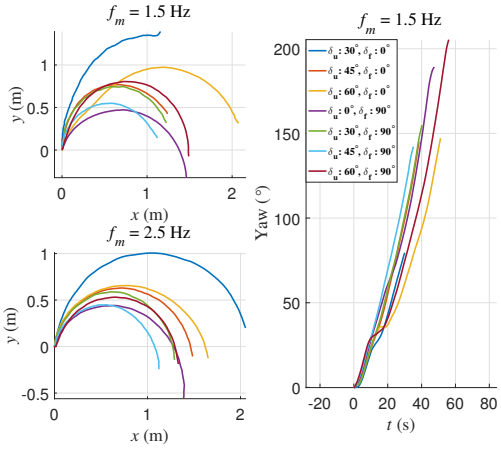

(a)

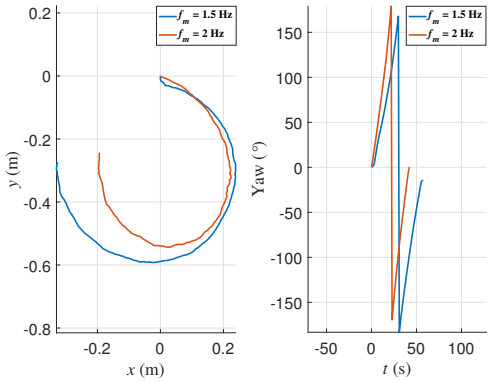

(b)

Fig. 6. Experimental data of turning mode based on MPF. (a) Flapping of unilateral flipper; (b) Flapping of bilateral flippers.

Fig. 5(b) denotes the results under different f_b when $\delta_u = 45°$. From the perspective of turning rate after the robot enters the steady state, the conclusion that the robot had better performances with higher frequency when the $\delta_f = 90°$ could be drawn.

2) MPF-based turning mode: There are two modes based on MPF, the results of which are illustrated in Fig. 6. The performance conditions of unilateral MPF-based mode are similar with the ones of BCF-based mode, other than smaller turning radii less than 1 BL. Interestingly, the robot could steer with a little turning radius as small as approximately 0.2-BL under bilateral MPF-based mode. Besides, as flapping frequency increases, the turning radius and turning rate were also optimized. Therefore, it is more suitable to apply the MPF-based mode in narrow area where the underwater

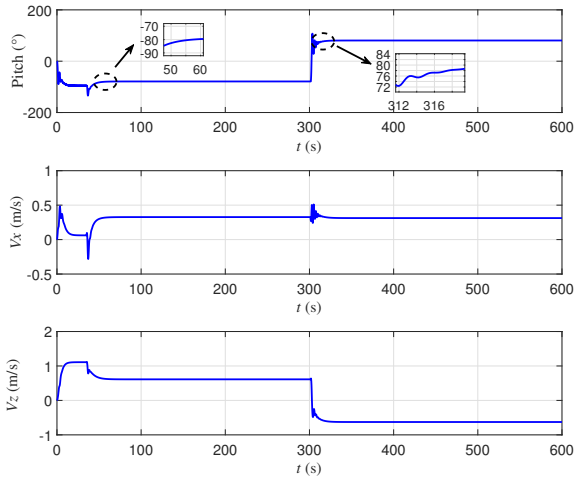

Fig. 7. Simulation results of vertical motion.

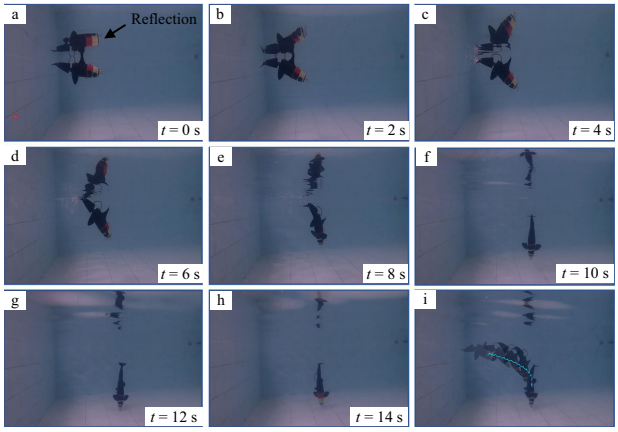

Fig. 8. Snapshot sequences of vertical motion.

operations often occur.

Through above analysis of various turning modes, the performances of the gliding robotic dolphin in horizontal motion are investigated. Every turning pattern has its own pros and cons. By combining these patterns, the robot can select different modes to achieve steering in various situations.

B. Experiments of Vertical Motion

According to the FSM, we carried out some simulations and experiments to verify the effectiveness of the framework. Fig. 7 indicates the simulation results in which the gliding robotic dolphin accomplishes a complete gliding round. Specially, compared with common gliding motion, the pitch angle reached much larger pitch angle more than 80° when the robot entered the steady gliding state. From the point of gliding angle, the gliding robotic dolphin could realize approximately 65°, which validated the effectiveness of proposed framework. In particular, before t = 35 s, the

robot dived under dolphin-like motion, and basically realized the vertical downward motion. Therefore, when there are tasks that requires the robot to dive with a vertical downward attitude, the dolphin-like motion can be selected. Actually, the attitude of robot in FSM-based gliding motion was also closer to the vertical downward.

Due to the size limitation of the test pool, we conducted some experiments of dolphin-like motion to rapidly adjust the attitude, which corresponded to the first and second stages in the FSM framework. The snapshot sequences are figured in Fig. 8. In particular, The *i*-th figure of Fig. 8 denotes the trajectory of vertical motion. As we can see, the gliding robotic dolphin took less than 10 s to complete the action. Besides, we also analyze the attitude information from IMU sensor, which indicates that the roll angle was basically the same in whole process. Moreover, from the point of pitch angle of IMU, there was a large acceleration since we set the waist and caudal angles to the opposite direction in the beginning, which resulted in a large pitch moment when starting the CPG flapping.

C. Discussion

Considering the gliding robotic dolphin has a shortage of capabilities in yaw motion, the performance in horizontal motion has been greatly improved with the aid of rudder and flipper. By virtue of the combination of five patterns, the gliding robotic dolphin can accomplish tasks better according to different scenarios. Compared with [14], there are two more BCF-based modes, which promotes the practical applications of the gliding robotic dolphin. Furthermore, an FSM framework is offered to achieve the vertical downward action and large gliding angle, which enhances the ability of vertical motion. However, for horizontal motion, the questions of how to combine and switch these patterns are of great need for better maneuverability. Similarly, in respect of the switching between the dolphin-like and gliding motions in the vertical plane, we simply reset the propulsive system as the transition way in this work, which may cause unstable attitude as shown in Fig. 7. Therefore, it is worth exploring the transition procedure between two motions.

V. Conclusions and Future Work

In this paper, we have investigated the 3-D motion maneuverability with the full consideration of horizontal and vertical motions. First, in an attempt to boost the turning performance of the gliding robotic dolphin, a rudder is designed and mounted on the belly. On the basis of the improvement, five turning modes are offered to analyze the turning capability. Second, a finite state machine framework is exploited to achieve the vertical downward action, further to explore the performances of the gliding robotic dolphin in vertical plane. Finally, multitudes of aquatic experiments are conducted and successfully validate the effectiveness of the rudder. The horizontal results and analysis obtained demonstrate the pros and cons of each pattern, which contributes to combine these modes to implement efficient path following. Meanwhile, the vertical experiments are also successfully realized, which are conducive to increase the diving ways of underwater vehicles. This study provides the valuable guidance for the real-world application of the gliding robotic dolphin.

The future work will focus on exploring the combination of turning modes by drawing on intelligent algorithms, such as reinforcement learning, further to achieve 2-D path planning and following in real-world environment.

References

[1] Z. Wu, J. Yu, Z. Su, and M. Tan, "An improved multimodal robotic fish modelled after *Esox lucius*," in *Proc. IEEE Int. Conf. Robot. Biomim.*, Shenzhen, China, Dec. 2013, pp. 516–521.

[2] X. Yang, Z. Wu, and J. Yu, "Design and implementation of a robotic shark with a novel embedded vision system," in *Proc. IEEE Int. Conf. Robot. Biomim.*, Qingdao, China, Dec. 2016, pp. 841–846.

[3] W. Wang and G. Xie, "Online high-precision probabilistic localization of robotic fish using visual and inertial cues," *IEEE Trans. Ind. Electron.*, vol. 62, no. 2, pp. 1113–1124, 2015.

[4] J. Yu, Z. Su, Z. Wu, and M. Tan, "An integrative control method for bio-inspired dolphin leaping: Design and experiments," *IEEE Trans. Ind. Electron.*, vol. 63, no. 5, pp. 3108–3116, 2016.

[5] J. Yu, Z. Su, M. Wang, M. Tan, and J. Zhang, "Control of yaw and pitch maneuvers of a multilink dolphin robot," *IEEE Trans. Robot.*, vol. 28, no. 2, pp. 318–329, 2012.

[6] J. Sherman, R. E. Davis, W. B. Owens, and J. Valdes, "The autonomous underwater glider 'Spray'," *IEEE J. Ocean. Eng.*, vol. 26, no. 4, pp. 437–446, 2001.

[7] C. C. Eriksen, T. J. Osse, R. D. Light, T. Wen, T. W. Lehman, P. L. Sabin, J. W. Ballard, and A. M. Chiodi, "Seaglider: A long-range autonomous underwater vehicle for oceanographic research," *IEEE J. Ocean. Eng.*, vol. 26, no. 4, pp. 424–436, 2001.

[8] Z. Wu, J. Liu, J. Yu, and H. Fang, "Towards a gliding robotic dolphin: Design, modeling, and experiments," *IEEE/ASME Trans. Mechatronics*, vol. 24, no. 1, pp. 260–270, 2019.

[9] Z. Wu, J. Yu, J. Yuan, M. Tan, and J. Zhang, "Mechatronic design and implementation of a novel gliding robotic dolphin," in *Proc. IEEE Int. Conf. Robot. Biomim.*, Zhuhai, China, Dec. 2015, pp. 267–272.

[10] J. Yuan, Z. Wu, J. Yu, and M. Tan, "Sliding mode observer-based heading control for a gliding robotic dolphin," *IEEE Trans. Ind. Electron.*, vol. 64, no. 8, pp. 6815–6824, 2017.

[11] Z. Wu, J. Yu, J. Yuan, M. Tan, and S. Qi "Gliding motion regulation of a robotic dolphin based on a controllable fluke," *IEEE Trans. Ind. Electron.*, 2019, DOI: 10.1109/TIE.2019.2913810.

[12] M. Nagai, *Thinking Fluid Dynamics with Dolphins*. Tokyo, Japan: Ohmsha, 2002.

[13] Z. Cao, F. Shen, C. Zhou, N. Gu, S. Nahavandi, and D. Xu, "Heading control for a robotic dolphin based on a self-tuning fuzzy strategy," *Int. J. Adv. Robot. Syst.*, vol. 13, no. 28, pp. 1–8, 2016.

[14] J. Liu, Z. Wu, J. Yu, and Z. Cao, "Flippers-based turning analysis and implementation of a dolphin robot," in *Proc. IEEE Int. Conf. Robot. Biomim.*, Macau, China, Dec. 2017, pp. 141–146.

[15] J. Wang, Z. Wu, Y. Yang, M. Tan, and J. Yu, "Spiraling motion of a gliding robotic dolphin based on the 3-D dynamic model," in *Proc. IEEE Int. Conf. Real-Time Comput. Robot.*, Kandima, Maldives, Aug. 2018, pp. 13–18.

[16] A. J. Ijspeert, A. Crespi, D. Ryczko, and J. M. Cabelguen. "From swimming to walking with a salamander robot driven by a spinal cord model". *Science*, vol. 315, no. 5817, pp. 1416–1420, 2007.

[17] J. Wang, Z. Wu, M. Tan, and J. Yu, "Controlling the depth of a gliding robotic dolphin using dual motion control modes," *Sci. China inf. Sci.*, 2019, DOI:10.1007/s11432-019-2671-y.